Ceramics International 46 (2020) 9741–9750

Contents lists available at ScienceDirect

Ceramics International

journal homepage: www.elsevier.com/locate/ceramint

Femtosecond laser pulse ablation characteristics of polymer-derived SiAlCN ceramics

Yigao Chen[a], Yejie Cao[a,*], Yiguang Wang[b], Ligong Zhang[c,**], Gang Shao[d], Jinfeng Zi[e]

[a] Science and Technology on Thermostructure Composite Materials Laboratory, Northwestern Polytechnical University, Xi'an, 710072, Shaanxi, China
[b] Institute of Advanced Structure Technology, Beijing Institute of Technology, Haidian District, Beijing, 100081, China
[c] State Key Laboratory of Luminescence and Applications, Changchun Institute of Optics, Fine Mechanics and Physics, Chinese Academy of Sciences, Changchun, 130033, Jilin, China
[d] School of Materials Science and Engineering, Zhengzhou University, Zhengzhou, 450001, China
[e] Xi'an MicroMach Technology Co., Ltd, Xi'an, 710072, Shaanxi, China

ARTICLE INFO

Keywords:
Femtosecond laser pulse
Polymer-derived ceramics
Ablation characteristics
Energy fluence

ABSTRACT

Polymer-derived ceramics (PDCs) are promising high-performance materials for various applications, yet their brittleness represents major drawback in their machining. Femtosecond laser pulse ablation is non-contact rapid processing method used in precision machining of PDCs. Herein, two laser parameters (laser energy fluence and rotational speed) were investigated to achieve laser–material interactions and machining characteristics via machine single circular lines, blind holes, and through-holes in polymer-derived SiAlCN ceramics. With the decrease in rotational speed, the morphology of single circular lines gradually roughened and heat-affected zone was produced. Varying ablation rates were obtained at different energy fluences. For blind holes, three different ablation regions were observed. As the energy fluence increased, blind holes gradually transformed into through-holes. Through-holes with near-cylindrical profiles and minimal collateral damage were obtained. Ablation debris deposited around through-holes were indicative of N release, breaking of Si–N and C–C bonds, and formation of SiO_x. Laser ablation of PDCs led to the formation of laser-induced surface structures, bubble pits, stripe structures, molten materials, and sphere-like particles.

1. Introduction

Polymer-derived ceramics (PDCs) are promising materials for microelectromechanical system applications owing to their excellent properties, including high-temperature stability, excellent oxidation/corrosion resistance, and semiconducting characteristics [1–3]. However, microelectromechanical systems based on PDCs fabricated by micro-casting, lithography, and photopolymerization [4–6] suffer from shrinkage and deformation issues [7]. In addition, these components can only be fabricated with limited thickness, and the pyrolysis process usually leads to residual stress, which can cause deformation and cracks [6]. However, PDCs become hard and brittle after pyrolysis, leading to machining difficulties by conventional machining methods. Ultra-fast laser machining has been applied in recent years in the fabrication of a wide variety of materials and shapes due to its high machining accuracy and quality [8]. Therefore, using the ultra-fast laser pulse seems suitable for the fine processing of PDCs.

Among the ultra-fast laser pulse, femtosecond pulse lasers are preferred in laser machining over their pico- and nanosecond counterparts commonly used for fine micromachining of metals, polymers, and ceramics [9–11]. When a femtosecond laser pulse is used in practical applications such as drilling, cutting, and scribing, the influence of the laser parameters on the machining characteristics on different materials must be assessed to obtain the desired results. Different laser–material interactions occur due to the differences in material properties [12]. Kamlage et al. [13] developed high-quality drilling processes for metals involving the generation of laser-induced metal vapor and small metal particles (debris), the transformation of laser pulses into light filaments, and low-fluence finishing. Different machining parameters were investigated in for femtosecond laser drilling of SiC/SiC composites, leading to a better quality surface morphology and machining results [14]. Similarly, given the different thermal properties of Al_2O_3 and AlN ceramics, different surface ablation morphologies were obtained using femtosecond laser micromachining [15,16]. Moreover, the possible removal of Al_2O_3 was induced by intense thermal stress with little melting, while the ablation of AlN was caused by melting and re-

* Corresponding author., Xi'an, Shaanxi, China.
** Corresponding author., Changchun, China.
E-mail addresses: caoyejie@nwpu.edu.cn (Y. Cao), zhanglg@ciomp.ac.cn (L. Zhang).

https://doi.org/10.1016/j.ceramint.2019.12.243
Received 6 December 2019; Received in revised form 25 December 2019; Accepted 27 December 2019
Available online 28 December 2019
0272-8842/

solidification. Nevertheless, since the amorphous features of PDCs differ significantly from those of metals and ceramics, their ablation behavior and morphologies under femtosecond laser pulse must be appropriately investigated to ensure the suitability of the technique.

Herein, Al-doped SiCN (SiAlCN) ceramics were selected as substrates owing to their low porosity and high oxidation/corrosion resistance at high temperatures [17,18]. The prism-rotary scanning mode is an important processing mode in industrial femtosecond laser devices, which was used to produce ring line and helical line scanning [19,20]. The machining characteristics of the prism-rotary scanning mode were investigated in detail when machining single circular lines, blind holes, and high-quality through-holes. Based on these laser machined patterns, the effects of the energy fluence and the rotational speed on the machining characteristics of SiAlCN ceramics were studied in detail, including the machining morphology and the underlying mechanism, thus fully assessing the ablation behavior of SiAlCN ceramics. The laser–material interactions and the effects of certain parameters of the femtosecond laser pulse on the fine processing of PDCs materials were also studied.

2. Experimental

2.1. Preparation of SiAlCN

Commercially available polysilazane (HTT1800, Kion, Huntingdon Valley, PA, USA) and aluminum isopropoxide ($Al[OCH(CH_3)_2]_3$) (Acros Organics, Thermo Fisher Scientific, USA) were used as starting materials (at a 90:10 wt ratio) to synthesize the SiAlCN precursor. The resulting mixture was continuously stirred at 120 °C for 6 h. Subsequently, dicumyl peroxide (2 wt%) was added to accelerate the cross-linking and heat curing processes; the produced bubbles were thoroughly removed under vacuum for 12 h. Translucent polymer rods were subsequently prepared by pouring the mixture into a Teflon mold and maintaining at 130 °C for 4 h. Discs of 1–1.5 mm in thickness were obtained by cutting the polymer rod with a low-speed diamond saw (SYJ-150, MTI Corporation, CA, USA) and pyrolyzed at 1000 °C for 4 h in a tube furnace (GXL-1100X, MTI Corporation) under ultrahigh-purity nitrogen protection. Fully dense SiAlCN ceramics of 0.5–1 mm in thickness and 9 mm in diameter were finally obtained. The SiAlCN ceramic wafers were polished (roughness below 10 nm) and cleaned with alcohol in an ultrasonic bath.

2.2. Laser machining experiments

A four-axis ultrafast laser micromachining instrument (LMM-50, Xi'an MicroMach Technology Co., Ltd., China) was used for the laser processing experiments. A regenerative amplified Yb-doped solid-state ultra-fast laser system was used to generate a femtosecond laser pulse with a wavelength of 1030 nm and a pulse duration of 290 fs The repetition rate was fixed at 100 kHz. The laser beam was applied to the sample surface with a focal length of 116.69 mm. The sample was mounted on a XYZ-translation stage and the laser beam was focused on the machining layer during the laser processing [19]. All the machining processes were carried out in ambient atmosphere.

Energy fluence is commonly used to assess the laser processing of materials. For a Gaussian laser beam, the peak fluence Φ_0 can be obtained as follows:

$$\Phi_0 = 2E_p/(\pi \times \omega^2) \quad (1)$$

where E_p and ω are the pulse energy and the spot radius, respectively [21].

Three processing patterns were employed herein using the prism-rotary scanning mode of laser machining, namely single circular lines, blind holes, and through-holes. In the case of single circular lines, the rotational speed varied from 400 to 2400 rpm for three different energy fluences (1.14, 2.28, and 4.57 J/cm^2). The maximum rotational speed limitation for this machine was 2400 rpm. The machining time was fixed to 0.25 s and the diameter of single circular lines was 415 μm. The diameter of the micro-holes was set at 350 μm, with a rotational speed of 2400 rpm and an energy fluence variation from 1.14 to 9.14 J/cm^2. The machining time for blind holes was 1 s. To achieve high-quality through-holes, the materials were removed by multilayer laser machining using the helical drilling strategy. In order to achieve sustained processing, the machining device was moved up and down to adjust the position of the laser beam along the processing axial direction. The feeding speed along the Z-axis direction was 50 μm/s.

2.3. Microstructure analysis

The morphologies of the laser-treated samples and the elemental composition of the debris were assessed by scanning electron microscopy (SEM; S4700, Hitachi, Japan) equipped with energy dispersion spectroscopy (EDS). X-ray photoelectron spectroscopy (XPS; K-Alpha, Thermo Scientific, USA) was used to detect the phase structure and chemical bond states of the laser-treated samples and untreated samples. Three-dimensional (3D) optical profilometry (ST400, NANOVEA, USA) and micro-computed tomography (MU2000-D, YXLON, German) were used to identify the morphologies of the single circular lines and cross-section features of the micro-holes.

3. Results and discussion

3.1. Effect of rotational speed on single circular lines

Rotational speed has an effect on the laser process and can be directly adjusted during experiments. Owing to the incubation effect of semiconductors, an ablation threshold fluence related to the pulse number incident on the sample can obtained [22]. For a Gaussian pulse profile, the effective laser pulse number (N_{eff}) is determined by the traverse velocity (ν), the pulse repetition rate (f), and the Gaussian laser spot radius (ω), according to the formula [21]:

$$N_{\text{eff}} = \sqrt{\pi/2} \times f\omega/\nu \quad (2)$$

where the laser pulse spacing is significantly lower than ω, f = 100 kHz is the repetition rate of the femtosecond laser, and the spot radius is of ~16.75 μm. Herein, for a rotational speed of 2400 rpm, N_{eff} was ~40, increasing to ~240 at a rotational speed of 400 rpm. N_{eff} is equivalent to the accumulated laser pulse fluence per unit length for a pulse with a Gaussian intensity profile, and therefore the machining behavior of femtosecond laser pulse depends on the rotational speed.

The single circular lines machined on the surface at different rotational speeds with an energy fluence of 2.28 J/cm^2 were observed (Fig. 1). The machining circular lines were 420 μm in diameter and were obtained at 0.25 s. The arc length increased with the rotational speed. At 2400 rpm, minor damage by laser machining was produced. The target SiAlCN ceramics quickly transformed into high-speed plasma following the absorption of laser energy, which was subsequently ejected thereby removing the materials. After laser machining, some ablated materials returned to the surface and re-condensed, and a minimal amount of debris found adhered onto the irradiated area (Fig. 1a). As the rotational speed decreased, more materials were ablated and more debris deposited on the surface of the irradiated area (Fig. 1b–d). Moreover, molten material adhered to the margin of the circular lines (Fig. 1d), possibly indicating that the ablation of SiAlCN ceramics was related to melting. Except for the molten material, the laser-induced stripes, covered with nanoparticles, were observed at the bottom of the circle lines oriented in parallel to the moving direction of the laser; this observation could be mainly related to the polarization of the laser beam, the energy fluence and N_{eff} [23–25]. Moreover, some cracks and irregular microstructures were observed at the bottom of the

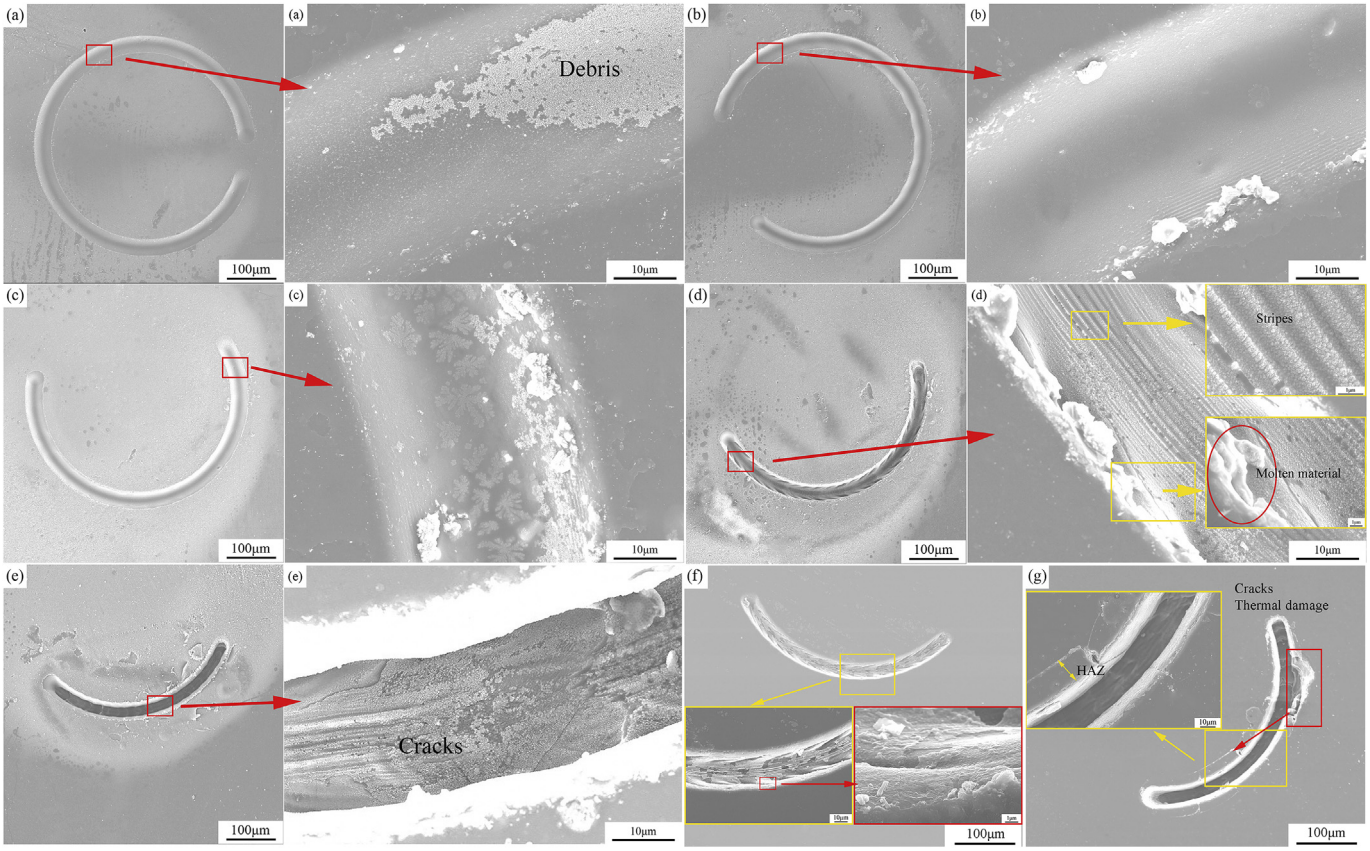

Fig. 1. SEM and 3D topography images of SiAlCN ceramics after single circular line machining with 2.28 J/cm^2 at different rotational speeds: **a** 2400 rpm, **b** 2000 rpm, **c** 1600 rpm, **d** 1200 rpm, and **e** 800 rpm. SEM images of SiAlCN ceramics after single circular line machining at 800 rpm at an energy fluence of **f** 1.14 J/cm^2 and **g** 4.57 J/cm.^{2}.

circle lines at low rotational speed of 800 rpm (Fig. 1e). Given the Gaussian distribution of the laser pulse, the energy distribution on the target surface is highly heterogeneous, with the ablation being focused on the center area of circle lines. Therefore, for excessively high N_{eff} values, cracks would be generated under the ablated layer as a result of thermal stress and thermal shock at the bottom of circular lines [26] (Fig. 1e). The region where the cracks formed, called heat-affected zone (HAZ), could be regarded as the result of excess heat caused by a high N_{eff}. The generation of HAZ reduces the machining quality in femtosecond laser precision processing. It has been suggested that the HAZ is formed when the accumulated laser fluence on the irradiated area exceeds a certain threshold. Therefore, in order to obtain the certain threshold energy, energy fluences of 1.14 J/cm^2 and 4.57 J/cm^2 were used to fabricate single circular lines at different rotational speeds in range of 400–2400 rpm. At an energy fluence of 1.14 J/cm^2 and the rotational speed of 800 rpm, the laser-irradiated area showed no cracks and minimal molten material adhered onto the edge (Fig. 1f). Therefore, at 1.14 J/cm^2, the HAZ did not form at rotational speeds higher than 800 rpm. Moreover, cracks and material fracture were observed when energy fluence increased to 4.57 J/cm^2 (Fig. 1g), showing more severe ablation behavior. In multipulse processing, the total amount of accumulated laser energy seems to be responsible for the ablation morphology characteristics. Of note, the ablated morphologies of circular lines were similar at the machining parameters of 1.14 J/cm^2, 800 rpm, and N_{eff} ~120 (Figs. 1f) and 2.56 J/cm^2, 1200 rpm, and N_{eff} ~80 (Fig. 1d). The energy fluence of 1.14, 2.56, and 4.57 J/cm^2 correspond to 5, 10, and 20 μJ/pulse, respectively. The total accumulated pulse energy is briefly calculated by N_{eff} × single pulse energy. Based on the ablated morphology for SiAlCN ceramics, when the laser energy is less than 600 μJ per unit area, single circular lines without HAZ were obtained, and 600 μJ were treated as a threshold for the formation of HAZ at these specific laser parameters. Therefore, in order to avoid collateral damage, high rotational speeds are preferred (e.g., 2400 rpm).

The depth and width of machined circular lines are two major measurement parameters to assess the degree of ablation. The 3D profiles of laser-machined single circular lines at 2.28 J/cm^2 with different rotational speeds were observed, and the width and depth of circular lines were defined (Fig. 2f). The width of circular lines was of ~35 μm and did not change with changing rotational speed. The depth of these Gaussian-profile circular lines was measured and plotted as a function of N_{eff} (Fig. 3). A linear relationship between the etching depth and N_{eff} was fitted, with the slope expressing the ablation rate. Ablation rates of 137, 206, and 320 nm/pulse were obtained for the three different energy fluences used herein (1.14, 2.28, and 4.57 J/cm^2, respectively). A good fitting was obtained for an energy fluence of 1.14 J/cm^2. The ablation rates showed nonlinear growth with the increasing energy fluence. At high energy fluence and low rotational speed, a greater amount of ablated material and debris were generated in the circular lines, forming a deep structure with HAZ. During laser processing, as the ablated depth increased, the laser pulse energy decreased due to greater absorption by restricted plasma and debris [21]. Thus, when the laser pulse arrives at the bottom of the circular lines, the energy was diminished, resulting in a reduced ablation rate. These deductions combined with the observed microstructure by SEM, suggested that a machined depth of under 10 μm would lead to the formation of high-quality single circle lines without HAZ for SiAlCN ceramics. Thus, for the machining of blind holes and through-holes, a rotational speed of 2400 rpm was suggested to achieve high-quality machining.

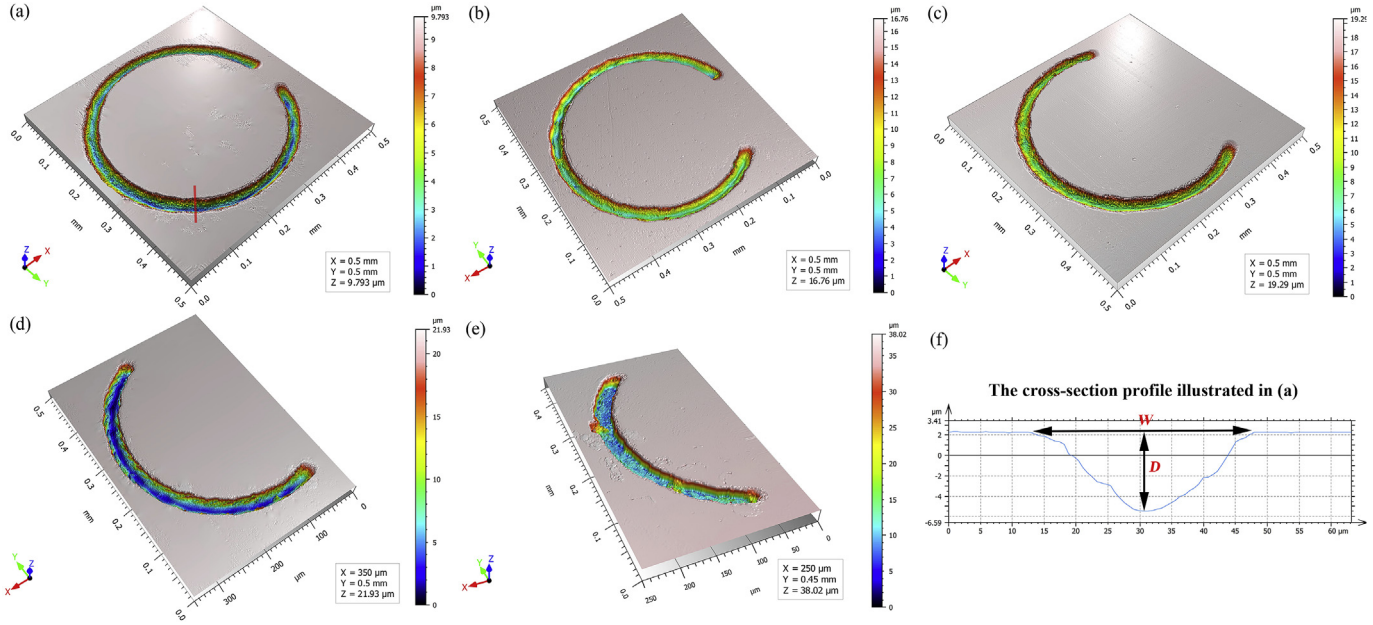

Fig. 2. 3D profiles of laser-machined single circular lines on SiAlCN ceramics with 2.28 J/cm^2 at different rotational speeds: **a** 2400 rpm, **b** 2000 rpm, **c** 1600 rpm, **d** 1200 rpm, and **e** 800 rpm **f** Definition of width and depth of circular lines.

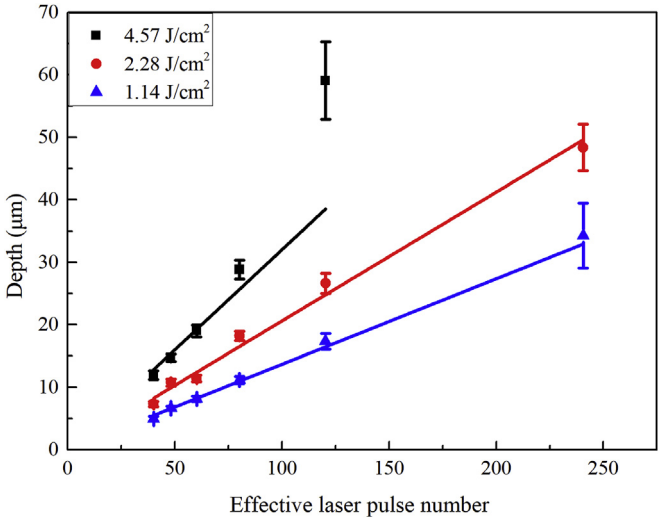

Fig. 3. Etching depths as a function of the effective laser pulse number for different energy fluences.

3.2. Effect of energy fluence for blind holes

In contrast to the machining of single circular lines, the helical line scanning was used to fabricate micro-holes, wherein the laser beam is scanned from the center to the margin [19]. With the aim to achieve SiAlCN ceramics with high-quality micro-holes, helical drilling was employed to machine micro-holes through layer-by-layer removal. SEM images of laser-machined blind holes (350 μm in diameter, 1 s, 2400 rpm) obtained with the helical line scanning and different energy fluences (1.14, 1.83, 2.28, 4.57, and 9.14 J/cm^2) were shown in Fig. 4. The ablated morphology of laser-induced periodic surface structures, molten materials, and cracks was observed following the formation of femtosecond laser-machined blind holes. The laser-irradiated area was divided into three sections: central, transition, and fringe regions (*I*, *II*, and *III*, respectively, in Fig. 4b). In the central region, a deep pit was generated at low energy fluence and deepened with increasing energy fluence (Fig. 4c). Especially at high energy fluences (Fig. 4e), the extended tip in the central region penetrated through the whole ceramic matrix, generating a through-hole. Once the blind holes were transformed into through-holes, the generated plasma and debris were directly ejected from the bottom of the SiAlCN ceramic, significantly increasing the ablation rate. Although a through-hole was fabricated at 9.14 J/cm^2, an unexpected HAZ with cracks was generated due to intense laser ablation. Moreover, the through-hole profile was non-cylindrical and coarse, indicating that the laser parameter is not appropriate for the machining of through-holes. Compared to the rapid variation of the depth in the central region, the profile of the transition region was relatively flat. At low energy fluences, laser-induced periodic surface structures were randomly generated at the transition region (Fig. 4a). EDS analysis showed that the layer was composed of Si, Al, C, N, and O, indicating the deposition of the debris on the unaffected layer (insert, Fig. 4a). However, at high energy fluences, these structures disappeared and the transition area became coarser due to severe ablation (Fig. 4c). In the fringe region, a large amount of molten material adhered at the periphery of the laser-machined blind holes (Fig. 4b). This molten material exhibited a columnar morphology, with the width increasing with the increase in energy fluence, and was shown to be composed of Si, Al, C, and O (inset Fig. 4d). During the ablation process, N is released, while other elements with relevant compositions are deposited. The existence of C and the increasing of C content (EDS data in Fig. 4a and d) were attributed to insufficient oxygen in ambient atmosphere during such rapid laser-machined processing. Thus, the ablated morphology of blind holes was obtained and their morphology evolution was helpful to understanding through-hole drilling.

3.3. Effect of energy fluence on through-hole drilling

Based on the above studies of single circular lines and blind holes, the fabrication of high-quality through-holes will require enough laser energy to remove the materials and decrease the degree of machining damage. Multiple layer removal was a more useful method to machine through-holes [20]. During laser processing, the focused laser beam moved along the Z axis. Therefore, the feeding speed was set at 50 μm/s for sufficient removal. The rotational speed was set at 2400 rpm in order to exert minimum thermal damage, and different energy fluences (1.14, 1.83, 2.28, 3.43, 4.57, 5.71, 6.86, 8.00 and 9.14 J/cm^2) were

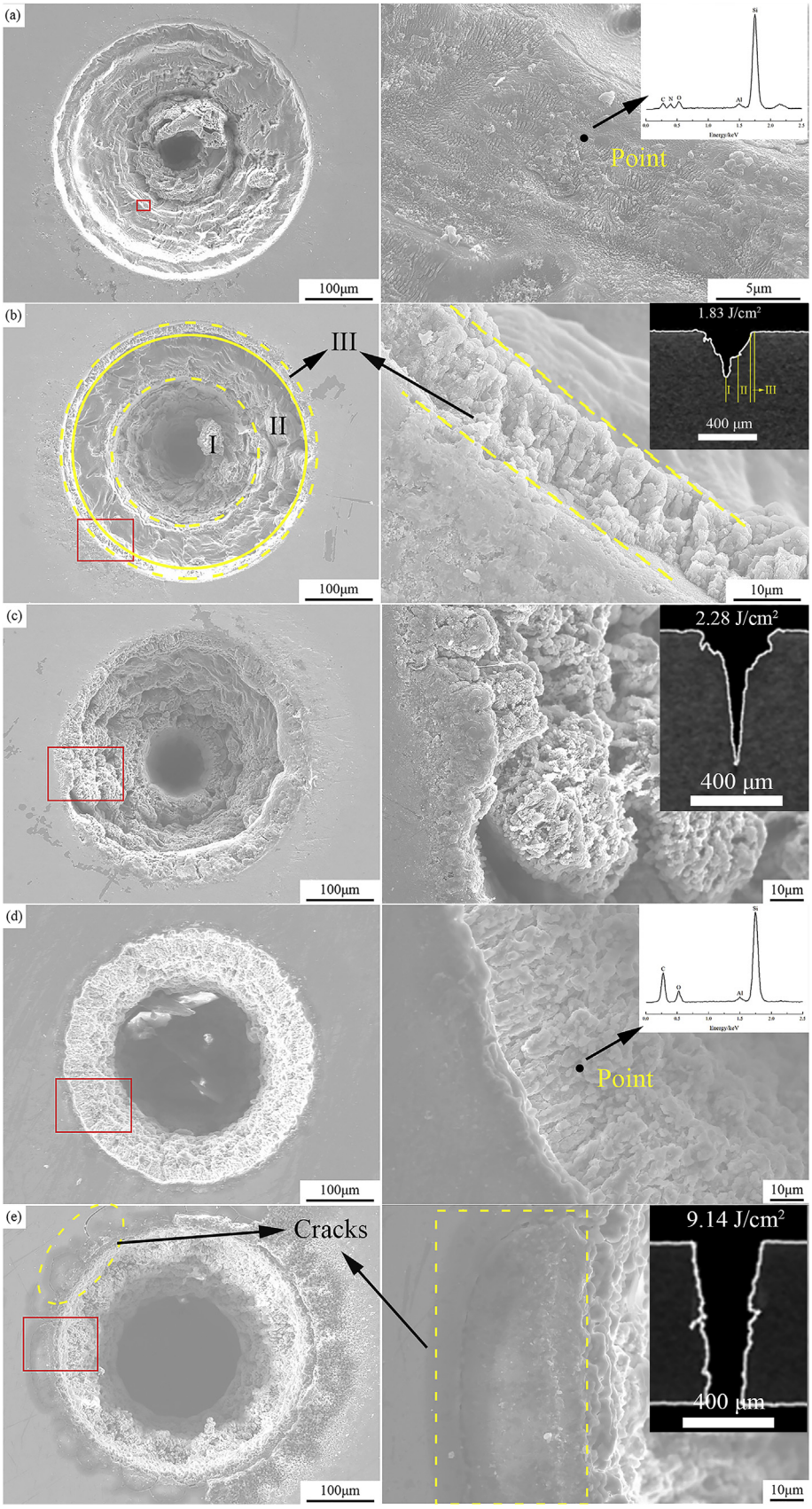

Fig. 4. SEM photos of the SiAlCN ceramics laser machined at different energy fluences: **a** 1.14 J/cm^2, **b** 1.83 J/cm^2, **c** 2.28 J/cm^2, **d** 4.57 J/cm^2, and **e** 9.14 J/cm^2. The second column includes zoomed images of images in the first column.

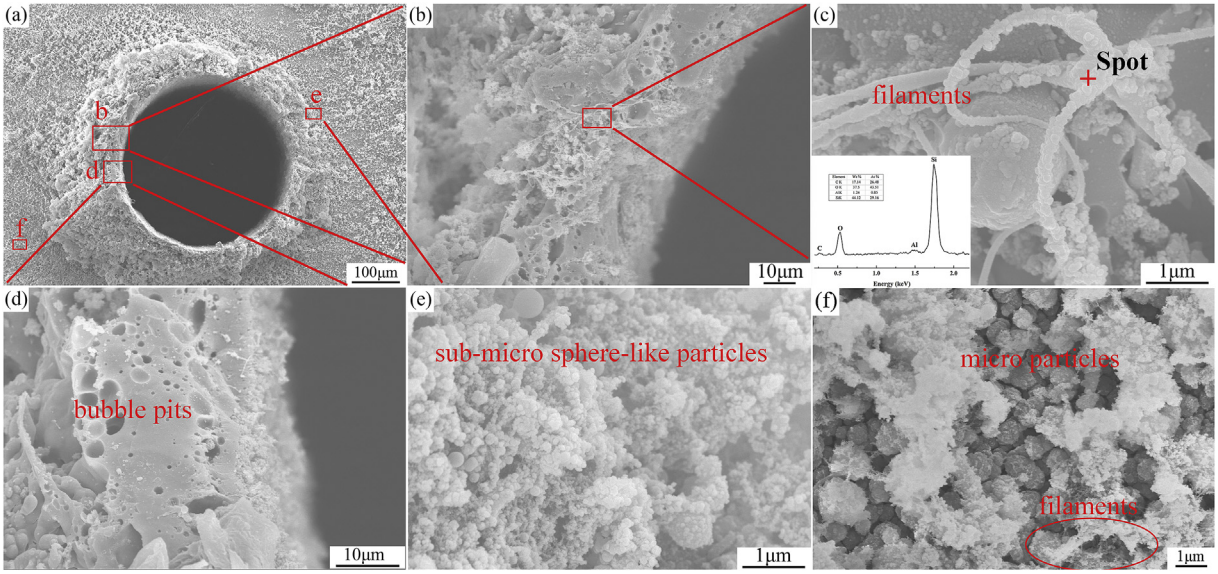

Fig. 5. SEM images and EDS patterns of the laser-drilled micro-holes without ultrasonic cleaning.

used. Micro-holes of 350 μm in diameter were machined via helical drilling without ultrasonic cleaning (Fig. 5). The formation of machining debris near the micro-holes was closely related to the femtosecond laser machining mechanism. SEM showed that the formed debris was present in three particular morphologies, namely sub-micro sphere-like particles, filaments, and bubble pits (Fig. 5); the latter were exclusively found near the holes. These bubble pits served as exhaust holes for gaseous species, such as NO and CO, produced by the reaction between plasma and oxygen [19]. The filaments and sphere-like particles were likely formed by SiO_2 or SiO in combination with other elements, including Al as assessed by EDS. The microstructure of the region away from the through-holes was composed of the micro sphere-like particles and filaments (Fig. 5f). Therefore, following laser processing, the N atom was abandoned and other elements were oxidized and deposited around the holes.

The characteristic XPS spectra of the surface of untreated SiAlCN ceramics and laser-treated samples showed that the peak position of N1s at 397 eV was only observed on the untreated surface, thus confirming the release of N during laser processing (Fig. 6). The decrease in relative intensity of the C1s peak indicated the rupture of the C–C bond. The deconvoluted XPS spectra of the C1s peak of the untreated SiAlCN ceramics and laser-treated surfaces showed four peaks at 283.4, 284.6, 285.4, and 287.7 eV, corresponding to C–Si [27], C–C (sp^2) [28], C–C (sp^3) [27], and C–N [29] bonds (Fig. 7). After laser machining, the Si–C bond and C–N bond disappeared, with peaks observed at 284.6, 285.4, and 288.5 eV, in line with C–C (sp^2), C–C (sp^3), and O–C═O [30] bonds. XPS high resolution spectra (Si 2p) of the untreated samples showed three peaks at 100.5, 102.1, and 103.6 eV, corresponding to Si–C [29], Si–N [31], and Si–O [29] bonds (Fig. 8). The Si–N bond was dominant and the content of Si–C and Si–O is relative less based on the microstructure of SiAlCN precursor [32], corresponding to the XPS result of Si 2p prior to laser treatment. Following femtosecond laser treatment, only two peaks were observed at 102.6 and 103.6 eV for SiO_x [27] and Si–O, indicating that the Si–N bond was ruptured and oxidized into Si–O bonds. Therefore, laser processing leads to the release of N, the formation of SO_2 and SiO_x, and the breaking of Si–N and C–C bonds.

The formation of laser-induced debris could be explained by the multi-photon absorption theory [33]. For semiconductors, the laser intensity (ca. 10^{13} W/cm^2) is sufficient to motivate plasmas from the irradiated surface with the laser pulse used herein (290 fs [34,35]. The laser consisted on a large amount of photons, which the energy of photons in a laser with a wavelength of 1030 nm is ca. 1.2 eV. According to the microstructure of SiAlCN ceramics and the XPS results above, the SiAlCN ceramics show mostly Si–N and C–C bonds with average binding energies of 355 and 347 kJ/mol, respectively (ca. 3.6 eV in both cases). Thus, SiAlCN ceramics require at least three photons to break the Si–N and C–C chemical bonds. Following laser irradiation, the amorphous SiAlCN ceramics structure is destroyed and transformed into free atoms, forming a high-speed plasma after

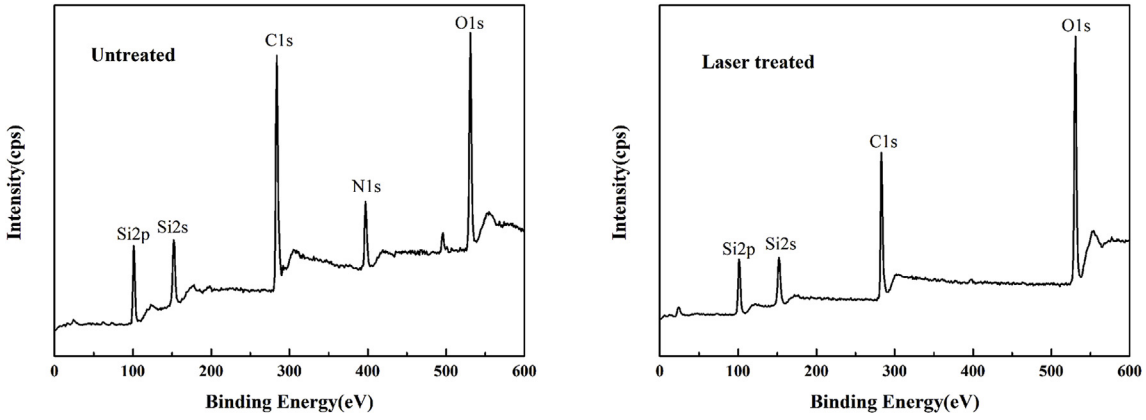

Fig. 6. XPS patterns of untreated and laser-treated SiAlCN ceramic surfaces.

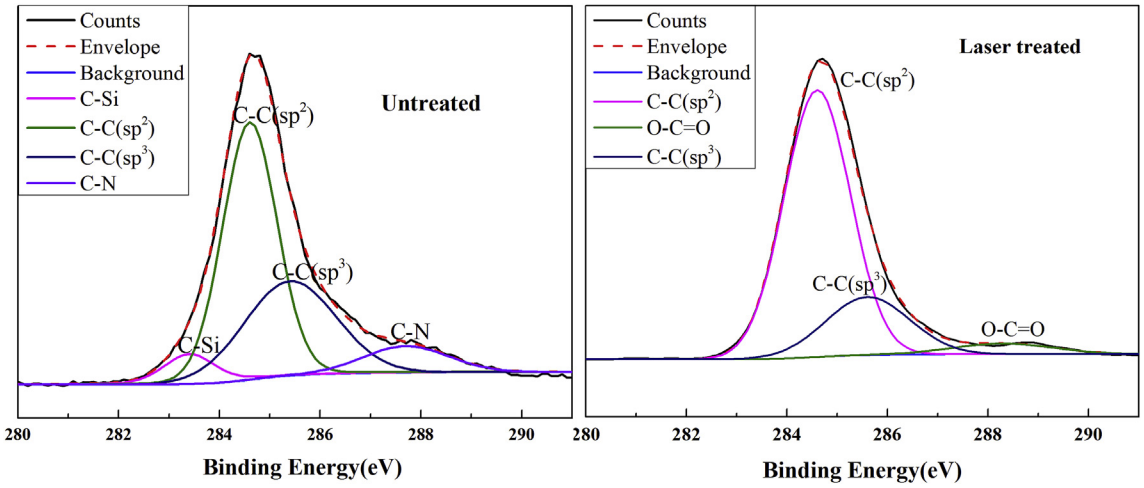

Fig. 7. XPS high resolution spectra (C 1s) of untreated and laser-treated SiAlCN ceramic surfaces.

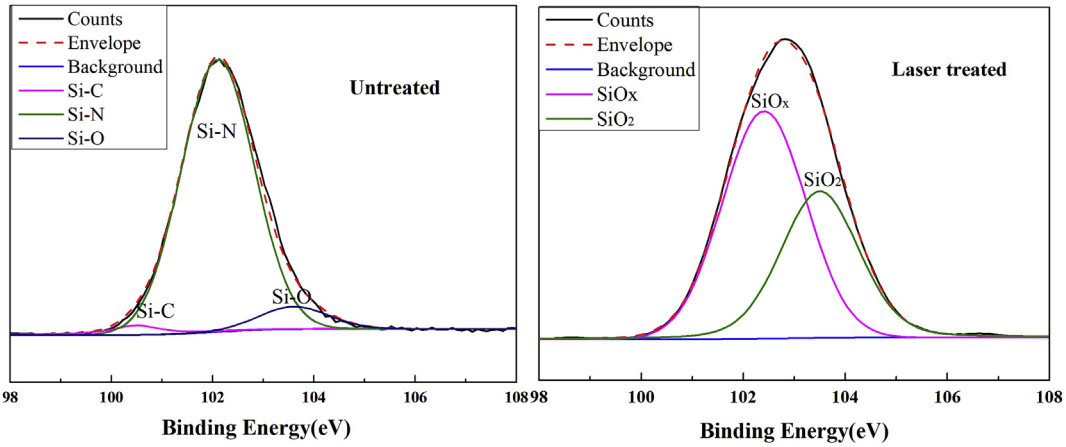

Fig. 8. XPS high resolution spectra (Si 2p) of untreated and laser-treated SiAlCN ceramic surfaces.

absorbing the laser energy. These plasmas are ejected from the irradiated area and subsequently react with O atoms of the surrounding air and the oxygen in SiAlCN, generating oxidation products such as SiO_x, CO_x, Al_2O_3, and NO_x. As expected, gaseous oxidation products such as CO_x and NO_x escape and SiO_x and Al_2O_3 condensate on the surface after the ablation process. Besides, given the inadequate oxidation during the laser process, some C atoms were retained and deposited in the debris.

Surface-deposited debris was easily removed after ultra-sonic cleaning due to their weak surface absorption force. The entry and exit sides of the through-holes and their two-dimensional (2D) cross-sections after ultrasonic cleaning were observed by SEM (Fig. 9). The diameter of through-holes was set at 350 μm. As clearly observed, a HAZ was unavoidably generated near the through-holes on the entry side. At low energy fluence shown in Fig. 9d, the diameter of the holes decreased from the top to the bottom, and the exit of the holes presented a coarse circular geometry with some deposited debris. The low energy fluences used herein were not sufficient to fabricate through-holes with a near-cylindrical profile. From the results of fabrication of blind holes (Fig. 4), the laser beam firstly penetrated through the SiAlCN ceramics in the center area, corresponding to the results in Fig. 9d. Thus, the exit holes were firstly formed in the center and enlarged with the increasing of energy fluence. When the energy fluence was higher than 4.57 J/cm^2, the diameter remained nearly unchanged along the depth of the hole, revealing a near-cylindrical profile. The diameter of holes on the entry and exit sides was measured and shown to increase with increasing energy fluence (Fig. 10), providing a wider exit for the debris to leave the through-holes. The changed diameter of holes in the entry side was the result of strong distortion and divergence on the laser beam, thereby increasing the intensity of the etching process around the entrance [36]. In addition, the through-holes showed a good circular geometry in both the entry and exit sides, shown in Fig. 9c and d. However, at an energy fluence of 9.14 J/cm^2, cracks generated at both the top and bottom sides as a result of the excessive accumulation of laser energy. Therefore, an energy fluence ranging from 5.72 and 8.00 J/cm^2 would be suitable for the formation of high-quality through-holes.

The microstructures of the HAZ around the holes were observed after drilling at 4.57 and 9.14 J/cm^2 (Fig. 10). At 4.57 J/cm^2 (Fig. 11a and b), the HAZ showed two different sections, namely a porous section and a thermal extension section. The porous section is always found at all machined through-holes. In the porous section, a large amount of bubble pits were generated at the HAZ, serving as escape channels for gaseous products during laser ablation. However, at 9.14 J/cm^2, some cracks generated in the thermal extension section were not expected (Fig. 11c), which caused the material to break (Fig. 11d). The formation of cracks is the result of high local stress induced by thermal shock at high energy fluence. The width of the HAZ was defined as the width of the porous section in low energy fluence or the maximum length of the crack at high energy fluence; further, the HAZ width was shown to increase with energy fluence (Fig. 11e). The generation of HAZ could be explained by a local heating effect [37]. During the femtosecond laser processing, the SiAlCN ceramics are heated with insufficient time between each pulse spacing for efficient cooling at high energy fluence. The heat subsequently diffuses into the surrounding area, inducing a

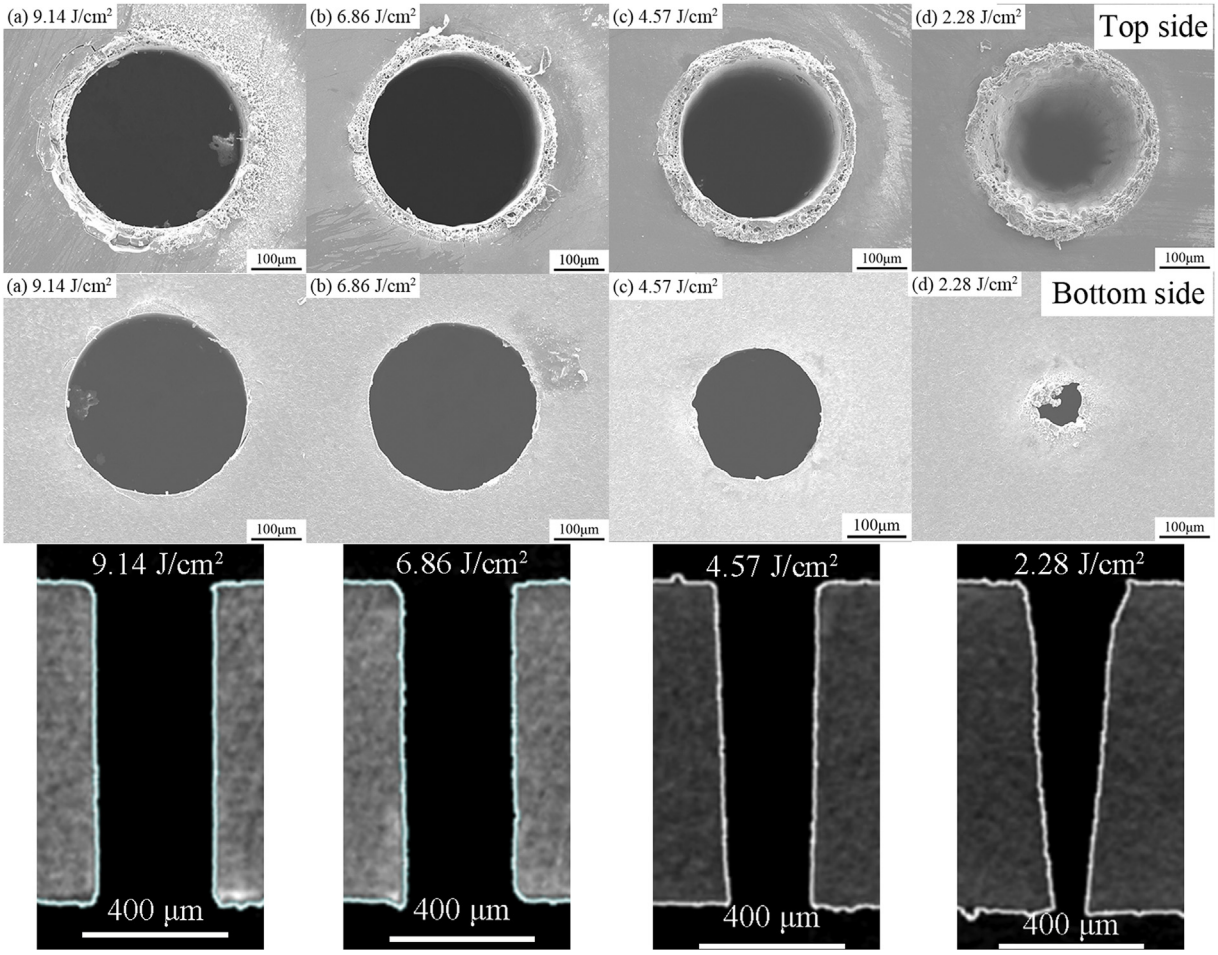

Fig. 9. Entry and exit sides and 2D cross-sections of laser-drilled holes at different energy fluences: **a** 9.14 J/cm^2, **b** 6.86 J/cm^2, **c** 4.57 J/cm^2, and **d** 2.28 J/cm.^{2}.

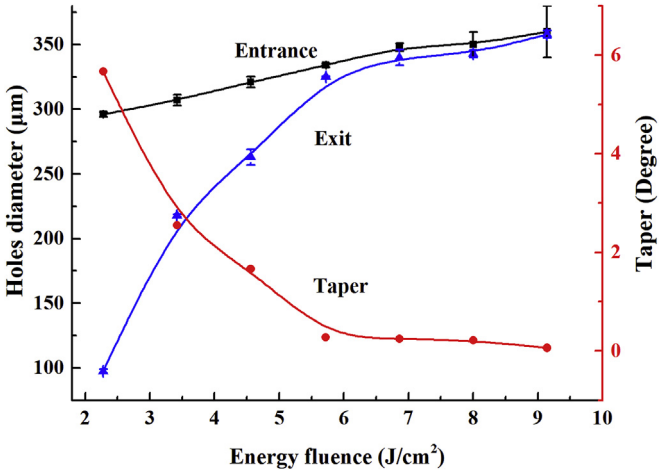

Fig. 10. Diameter of the holes and taper as a function of energy fluence.

local heating effect in the inner layer. The porous section or cracks were then generated due to the excessive accumulated laser energy. Prior to the formation of through-holes, the laser-induced plasma and debris are only sputtered from the entry side, which is restricted in deep and narrow spaces. More laser energy is absorbed by the restricted plasma and debris; they converted into heat and then transfer to the hole's sidewall in such deep structures, generating a HAZ or even cracks on the entry side. Once through-holes have been formed, the laser-induced plasma and debris are directly removed along the direction of laser beam, with the local heat effect no longer being important. Therefore, the HAZ with porous section is not found on the exit side (Fig. 9).

4. Conclusions

Herein, single circular lines, blind holes, and through-holes were fabricated on SiAlCN ceramics by a femtosecond laser pulse. The machining characteristics and processing quality were closely related to the energy fluence and rotational speed. For single circular lines, an absorbed total laser energy of less than 600 μJ and an ablated depth of less than 10 μm were suggested to reduce the debris, laser-induced stripes, molten material, and cracks. Ablation rates of 137, 206, and 320 nm/pulse at 1.14, 2.28, and 4.57 J/cm^2 were obtained. For blind holes, three different ablation regions were observed. The evolution from blind holes to through-holes was demonstrated with the preferential extension of the pit in the central region with increasing energy fluence. During through-hole drilling, a HAZ with a porous section and thermal extension section was observed, and its width increased with increasing energy fluence. In order to obtain high-quality through-holes, a rotation speed of 2400 rpm and energy fluences of between 5.72 and 8.00 J/cm^2 are suggested to ensure the machining quality. A laser–material interaction was demonstrated by the presence of laser-induced debris, which appeared in three morphologies, namely submicro sphere-like particles, filaments, and bubble pits. EDS and XPS showed that N was released, Si–N, Si–C and C–C bonds were broken, and SiO_x, C and Al_2O_3 were deposited. The present study plays a vital role in understanding the processing of laser-machined PDCs and guiding the precision machining of these materials.

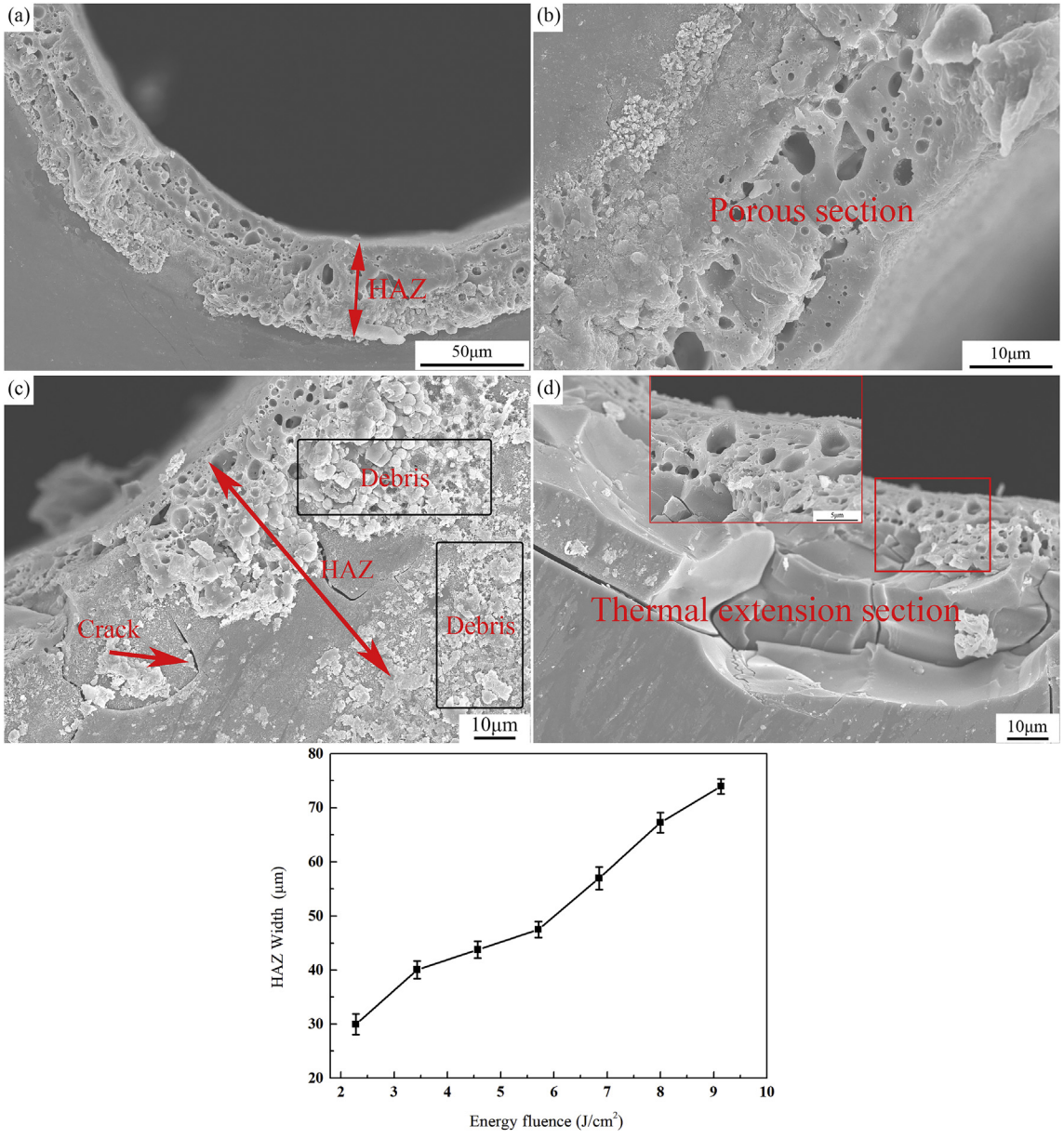

Fig. 11. Microstructures of the HAZ at different energy fluences: **a**, **b** 4.57 J/cm^2, **c**, **d** 9.14 J/cm^2 **e** The relationship between the HAZ width and energy fluence.

Declaration of competing interest

We state the work described here is an original research that has not been submitted elsewhere for publication, in whole or in part. No conflict of interest exits in the submission of this manuscript, and manuscript is approved by all authors for publication.

Acknowledgement

The authors acknowledge the support of the National Key Basic Research Program of China [grant number 2015CB057400]; the CAS equipment project [grant number YJKYYQ 20180045]; Natural Science Foundation of Shaanxi Province of China [grant number 2019JQ-540]; the Fundamental Research Funds for the Central Universities.

References

[1] P. Colombo, G. Mera, R. Riedel, G.D. Sorarù, Polymer-derived ceramics: 40 years of research and innovation in advanced ceramics, J. Am. Ceram. Soc. 93 (2010) 1805–1837.

[2] D. Freese, G. Shao, C.Y. Xu, Polymer–derived ceramic sensors for temperature measurement in harsh environment, ASME Turbo Expo 2013: Turbine Technical Conference and Exposition (pp.V004T02A011).

[3] J.B. He, Y.J. Cao, Y.X. Zhang, Y.G. Wang, Mechanical properties of ZrB_2–SiC ceramics prepared by polymeric precursor route, Ceram. Int. 44 (2018) 6520–6526.

[4] L.A. Liew, W. Zhang, V.M. Bright, L.N. An, M.L. Dunn, R. Raj, Fabrication of SiCN ceramic MEMS using injectable polymer–precursor technique, Sens. Actuators A Phys. 89 (2001) 64–70.

[5] Y.P. Liu, L.A. Liew, R.L. Luo, L.N. An, M.L. Dunn, V.M. Bright, J.W. Daily, R. Raj, Application of microforging to SiCN MEMS fabrication, Sens. Actuators A Phys. 95 (2002) 143–151.

[6] L.A. Liew, Y.P. Liu, R.L. Luo, T. Cross, L.N. An, V.M. Bright, M.L. Dunn, J.W. Daily, R. Raj, Fabrication of SiCN MEMS by photopolymerization of pre–ceramic polymer, Sens. Actuators A Phys. 95 (2002) 120–134.

[7] R. Riedel, G. Passing, H. Schönfelder, R.J. Brook, Synthesis of dense silicon–based ceramics at low temperatures, Nature 355 (1992) 714–717.

[8] J. Cheng, C.S. Liu, S. Shang, D. Liu, W. Perrie, G. Dearden, K. Watkins, A review of ultrafast laser materials micromachining, Opt. Laser. Technol. 46 (2013) 88–102.

[9] A. Ancona, S. Döring, C. Jauregui, F. Röser, J. Limpert, S. Nolte, A. Tünnermann, Femtosecond and picosecond laser drilling of metals at high repetition rates and average powers, Opt. Lett. 34 (2009) 3304–3306.

[10] X. Zhu, A.Y. Naumov, D.M. Villeneuve, P.B. Corkum, Influence of laser parameters and material properties on micro drilling with femtosecond laser pulses, Appl. Phys. A Mater. 69 (1999) S367–S371.

[11] Y. Zhang, Y.Q. Wang, J.Z. Zhang, Y.S. Liu, X.J. Yang, Q. Zhang, Micromachining

features of TiC ceramic by femtosecond pulsed laser, Ceram. Int. 5 (2015) 6525–6533.
[12] M.V. Allmen, A. Blatter, Laser-beam Interactions with Materials: Physical Principles and Applications, second ed., Springer Science & Business Media, Berlin, 2013.
[13] G. Kamlage, T. Bauer, A. Ostendorf, B.N. Chichkov, Deep drilling of metals by femtosecond laser pulses, Appl. Phys. A Mater. 77 (2003) 307–310.
[14] Y.S. Liu, R.H. Zhang, W.N. Li, J.X.J. Yang, L.F. Cheng, L.T. Zhang, Effect of machining parameter on femtosecond laser drilling processing on SiC/SiC composites, Int. J. Adv. Manuf. Technol. 96 (2018) 1–17.
[15] S.H. Kim, I.B. Sohn, S. Jeong, Ablation characteristics of aluminum oxide and nitride ceramics during femtosecond laser micromachining, Appl. Surf. Sci. 255 (2009) 9717–9720.
[16] B.C. Chen, C.Y. Ho, M.Y. Wen, C.S. Chen, C. Ma, Y.H. Tsai, Ultrashort–laser–pulse machining characteristics of aluminum nitride and aluminum oxide, Ceram. Int. 41 (2015) S191–S196.
[17] Y.G. Wang, L.N. An, Y. Fan, L.G. Zhang, S. Burton, Z.H. Gan, Oxidation of polymer–derived SiAlCN ceramics, J. Am. Ceram. Soc. 88 (2010) 3075–3080.
[18] A. Dhamne, W.X. Xu, B.G. Fookes, Yi Fan, L.G. Zhang, B. Sarah, J.Z. Hu, J. Ford, L.N. An, Polymer–ceramic conversion of liquid polyaluminasilazanes for SiAlCN ceramics, J. Am. Ceram. Soc. 88 (2010) 2415–2419.
[19] Y.S. Liu, C.H. Wang, W.N. Li, L.T. Zhang, X.J. Yang, G.H. Cheng, Q. Zhang, Effect of energy density and feeding speed on micro–hole drilling in C/SiC composites by picosecond laser, J. Mater. Process. Technol. 214 (2014) 3131–3140.
[20] F. Dausinger, H. Hügel, V. Konov, Micromachining with ultrashort laser pulses: from basic understanding to technical applications, Proc. SPIE 5147 (2003) 106–115.
[21] A. Borowiec, H.K. Haugen, Femtosecond laser micromachining of grooves in indium phosphide, Appl. Phys. A Mater. 79 (2004) 521–529.
[22] J. Bonse, J.M. Wrobel, J. Krüger, W. Kautek, Ultrashort-pulse laser ablation of indium phosphide in air, Appl. Phys. A Mater. 72 (2001) 89–94.
[23] T.H.R. Crawford, A. Borowiec, H.K. Haugen, Femtosecond laser micromachining of grooves in silicon with 800 nm pulses, Appl. Phys. A Mater. 80 (2005) 1717–1724.
[24] F. Costache, M. Henyk, J. Reif, Modification of dielectric surfaces with ultra–short laser pulses, Appl. Surf. Sci. 186 (2002) 352–357.
[25] A.Y. Vorobyev, C. Guo, Direct femtosecond laser surface nano/microstructuring and its applications, Laser Photonics Rev. 7 (2013) 385–407.
[26] D. Sciti, A. Bellosi, Laser–induced surface drilling of silicon carbide, Appl. Surf. Sci. 180 (2001) 92–101.
[27] H.F. Li, S. Dimitrijev, D. Sweatman, H.B. Harrison, P. Tanner, B. Feil, Investigation of nitric oxide and Ar annealed SiO_2/SiC interfaces by x-ray photoelectron spectroscopy, J. Appl. Phys. 86 (1999) 4316.
[28] C. Hinnen, D. Imbert, J.M. Siffre, P. Marcus, An in situ XPS study of sputter-deposited aluminium thin films on graphite, Appl. Surf. Sci. 78 (1994) 219–231.
[29] K. Yamamoto, Y. Koga, S. Fujiwara, XPS studies of amorphous SiCN thin films prepared by nitrogen ion-assisted pulsed-laser deposition of SiC target, Diam. Relat. Mater. 10 (2001) 1921–1926.
[30] F. Bodino, G. Baud, M. Benmalek, J.P. Besse, H.M. Dunlop, M. Jacquet, Alumina coating on polyethylene terephthalate, Thin Solid Films 241 (1994) 21–24.
[31] T. Hagio, A. Takase, S. Umebayashi, X-ray photoelectron spectroscopic studies of β-sialons, J. Mater. Sci. Lett. 11 (1992) 878–880.
[32] F. Berger, M. Weinmann, F. Aldinger, K. Müller, Solid-state NMR studies of the preparation of Si–Al–C–N ceramics from aluminum-modified polysilazanes and polysilycarbodiimides, Chem. Mater. 16 (2004) 919–929.
[33] A.A. Serafetinides, C.D. Skordoulis, M.I. Makropoulou, A.K. Kar, Picosecond and subpicosecond visible laser ablation of optically transparent polymers, Appl. Surf. Sci. 135 (1998) 276–284.
[34] X. Zeng, X.L. Mao, R. Greif, R.E. Russo, Experimental investigation of ablation efficiency and plasma expansion during femtosecond and nanosecond laser ablation of silicon, Appl. Phys. A Mater. 80 (2005) 237–241.
[35] P. Lorazo, L.J. Lewis, M. Meunier, Short–pulse laser ablation of solids: from phase explosion to fragmentation, Phys. Rev. Lett. 91 (2003) 225502.
[36] K.X. Pham, T. Rie, I. Yoshiro, Trepanning drilling of microholes on cemented tungsten carbide using femtosecond laser pulses, J. Laser Appl. 24 (2012) 1095–1101.
[37] J.K. Chen, W.P. Latham, J.E. Beraun, The role of electron–phonon coupling in ultrafast laser heating, J. Laser Appl. 17 (2005) 63–68.